fishes

MDPI

Article

A Mutation in Damage-Specific DNA Binding Protein One (ddb-1) Underlies the Phenotype of the No-Marginal-Zone (nmz) Mutant Zebrafish

Kailey Jerome, Aria Gish, Taylor Aakre, Taylor Brend, Mara Kate Grenier, Christina L. Johnson, Jaxon Gronneberg, Colin K. O'Neill, Lucas Radermacher and Tristan Darland *

Biology Department, University of North Dakota, Grand Forks, ND 58202, USA; tayaakre@gmail.com (T.A.); taylorbrend123@gmail.com (T.B.); lucas.radermacher@gmail.com (L.R.)
* Correspondence: tristan.darland@und.edu

Abstract

The ciliary marginal zone (CMZ) is a region in the peripheral-most retina that displays ongoing retinogenesis during growth and expansion of the eye in adulthood. While there is evidence that this capacity also exists in birds and mammals, it is far more robust in fish and amphibians. The process of CMZ retinogenesis is essentially equivalent to that seen early in the central retina; however, its regulation is not fully understood. In a previous study, we attempted to uncover novel regulatory genes by using a forward genetics screen in zebrafish, looking for recessive CMZ mutants. One of the mutants found was called *no marginal zone* (*nmz*). The *nmz* mutant showed relatively normal central retina development, but a lack of cells in the CMZ by 5 days post fertilization (dpf). Mapping, genomic sequencing, and complementation analysis using a second mutant line (*m863*) isolated in another laboratory showed that a mutation in damage-specific DNA binding protein-1 (ddb-1) gene underlies the phenotype seen in *nmz*. BrdU labeling suggested that later expansion and differentiation of CMZ retinal progenitors is more affected by ddb-1 loss than the earlier process of stem cell asymmetric division. As was seen for the *m863* mutant and in other studies with mice, one profound effect of ddb-1 loss in *nmz* was the upregulation in expression of tp53 and several of its downstream effectors. Several important genes important in CMZ retinogenesis are also downregulated in the *nmz* mutant. The change in gene expression would suggest that ddb-1 loss leads to increased cell cycle disruption and apoptosis at the expense of CMZ retinogenesis. While homozygosity is lethal, heterozygous fish appear to be completely normal in morphology, visual function, and behavior.

Keywords: ciliary marginal zone; CMZ; ddb-1; eye development; retinal stem cell

Key Contribution: This study adds to previous studies showing the importance of the ddb-1 gene in the maintenance of neural stem cell populations. In the absence of this gene, retinal stem cells in the CMZ go through cell cycle disruption and apoptosis, failing to produce new retinal tissue. As in previous reported studies of ddb-1 loss, cell death appears related to an elevated expression of tp53-regulated pathways. Heterozygosity for the ddb-1 null mutation does not appear to affect behavior or vision.

check for updates

Academic Editor: Laura Sánchez

Received: 2 September 2025
Revised: 14 October 2025
Accepted: 16 October 2025
Published: 22 October 2025

Citation: Jerome, K.; Gish, A.; Aakre, T.; Brend, T.; Grenier, M.K.; Johnson, C.L.; Gronneberg, J.; O'Neill, C.K.; Radermacher, L.; Darland, T. A Mutation in Damage-Specific DNA Binding Protein One (ddb-1) Underlies the Phenotype of the No-Marginal-Zone (nmz) Mutant Zebrafish. *Fishes* **2025**, *10*, 539. https://doi.org/10.3390/fishes10110539

Copyright: © 2025 by the authors. Licensee MDPI, Basel, Switzerland. This article is an open access article distributed under the terms and conditions of the Creative Commons Attribution (CC BY) license (https://creativecommons.org/licenses/by/4.0/).

1. Introduction

The ciliary marginal zone (CMZ) is a stem cell niche found in teleost fish and amphibians that generates retinal tissue as the eye and visual field grows, even in adulthood [1,2]. The CMZ is an annulus of cells found at the periphery of the retina. Retinal stem cells at the lateral edge of the annulus go through asymmetric division and generate a population of retinal progenitors that finally differentiate as a clonal wedge that includes all mature retinal cell types. CMZ-generated cells sequentially express neurogenic and neurodifferentiation genes implicated in central retinal development and other neural stem cell niches [3,4]. Regulation of the CMZ is still not fully understood, though its proximity to other eye structures, including the retinal pigmented epithelium (RPE), retinal vasculature, and lens, suggests coordinated growth by secreted proteins and/or cell–cellcell-cell contact.

While present in most clades of aquatic poikilothermic vertebrates, the CMZ has been lost in homeothermic terrestrial vertebrates [2]. However, it has been established that the nonpigmented ciliary epithelium in mammals and birds does have neural stem cell potential [4–6]. There has thus been an ongoing effort to understand the regulation of retinal stem cell populations in fish and amphibians to perhaps provide novel strategies for repairing retinal injury and treating degenerative retinal diseases in humans.

Forward genetics using zebrafish has been successfully used to uncover novel regulatory genes and pathways underlying several developmental processes [7–9]. In forward genetics approaches, male zebrafish are exposed to a mutagen and are bred to normal females to generate F_1 fish that can be screened for dominant mutations. Outcrossing the F_1 fish generates F_2 mutant lines that can be screened for recessive mutations after sibling in-crosses. In a previous study, we used mutagenized zebrafish that were screened for recessive mutations affecting eye morphology and function [10]. Similarly to a later, more extensive screen by another group [11], we looked for small eyes that showed relatively normal central retinal histology but lacked a CMZ. In the present study, we characterize one of these eye mutants that we called "*no marginal zone*" (*nmz*). We mapped the mutation and identified the likely mutation underlying *nmz* through genomic sequencing. The implicated gene codes for the damage-specific DNA binding protein-1 (ddb-1) were determined. Complementation analysis using a distinct ddb-1 mutant fish line, *m863*, isolated in another laboratory [12], was used to verify the same defective gene in *nmz*.

The ddb-1 protein binds to damaged DNA and initiates repair [13,14]. The ddb-1 protein also complexes with Cullin 4 A and associated factors to form a ubiquitin ligase complex called CRL4. The CRL4 complex ubiquitinates several target proteins, marking them for proteasome degradation. In this way, ddb-1 plays a critical role regulating target protein stability and progression progress through the cell cycle. Among potential CRL4 targets is the Tp53 protein, a transcriptional activator of several genes that regulate cell cycle progression and apoptosis [15–17]. Several cell stressors downregulate CRL4 activity, which coincides with increased Tp53 levels. The increased Tp53 triggers cell cycle arrest and/or cell death, depending on the developmental context [12,18,19]. Similarly to what has been found by others [12], our results suggest that ddb-1 also plays a role in CMZ neurogenesis. However, certain caveats of using forward genetics in zebrafish for this application necessitate caution in drawing any firm conclusions. Our study also provides additional support for the well-established model of CMZ neurogenesis and perhaps reveals certain nuances that add to this model.

2. Methods

2.1. Fish Husbandry and Mutagenesis

Zebrafish were maintained in the facility at the University of North Dakota according to standard Institutional Animal Care and Use Committee recommendations (IACUC2307-

0047 and -48). Fish were raised and maintained in stand-alone fish racks (Aquatic Habitats, Pentair Aquatics, Apopka, FL, USA). The fish were fed twice daily and kept in a constant 14-h-on, 10-h off, light cycle. All behavioral and visual experiments were conducted in the main facility room, which was maintained at 28 °C, where the home tanks were kept.

The *nmz* mutant was originally generated via an ethyl-nitroso-urea (ENU) mutagenesis and screening experiment at Harvard University, as described previously [10]. The *nmz* mutation was mapped to LG 18 on the MGH panel using simple sequence length polymorphism (SSLP) analysis, which has been described by others [20,21]. The *m863* mutant was a generous gift from the Driever Laboratory in Freiberg Germany [12].

2.2. Morphological Analysis, Histology, Electron Microscopy (EM), BrdU Labeling and Immunohistochemistry

Zebrafish larvae were imaged and morphologically measured using a Leica dissecting microscope (M165FC), Leica camera (DFC310FX), and Leica LAS4.1.0 image analysis software suite (Leica Microsystems, Heerbrugg, Switzerland). Histology and electron microscopy (EM) were conducted as described previously [22,23]. Briefly, 5 dpf larvae were anesthetized in tricaine and placed in a primary fixative (1% paraformaldehyde and 4% glutaraldehyde dissolved in PBS with 3% sucrose and 0.15 mM $CaCl_2$). After rinsing, the fixed larvae were dehydrated in an ethanol series followed by propylene oxide and then embedded in Epon-Araldite resin (Electron Microscopy Sciences, Hatfield, PA, USA). For light microscope examination, 1 µm sections were cut on an ultramicrotome and stained with 1% methylene blue and 1% azure blue buffered in borax. Sections were visualized on a Leica compound microscope (DM500B), Leica camera (DFC480) and the Leica LAS3.7 image analysis software suite (Leica Microsystems, Heerbrugg, Switzerland). For EM, secondary fixation with 1% osmium tetroxide was used after primary fixation. After rinsing, 80 nm sections were cut on an ultramicrotome, mounted onto grids, and further treated with lead citrate and uranyl acetate. Sections were visualized on the Hitachi transmission EM in the Harvard University core facility. For BrdU labeling, 3 dpf larvae were incubated for 24 h in 10 mM BrdU. The fish were rinsed at 4 dpf and allowed to grow for another 24 h before fixation and immunolabeling with an anti-BrdU antibody (Santa Cruz Biotechnology, Inc., Dallas, TX, USA) and the 1D1 antibody that labels rod photoreceptors (a generous gift from Dr. James Fadool at Florida State University).

2.3. Genomic and Transcriptomic Sequencing and Bioinformatics

A single adult male fish heterozygous for *nmz* and a single male homozygous wild-type sibling were sacrificed, and the livers were removed. Genomic DNA was purified from the liver tissue using a DNeasy kit (Qiagen, Germantown, MD, USA). The purified DNA was then sent to Admera Health Biopharma Services (South Plainfield, NJ, USA) through the Genohub platform. Admera performed quality control using gDNA TapeStation (Agilent Technologies, Santa Clara, CA, USA), library preparation using a KAPA Hyper Prep kit (Roche Technologies, Basel, Switzerland), and Illumina sequencing, the latter resulting in 80 million bidirectional reads of 150 bp. Admera also performed bioinformatic analysis, including read mapping and identification of single-nucleotide polymorphisms (SNPs) that varied between the two fish using BWA-MEM (v.0.7.17) software. Analysis using GATK HaplotypeCaller (v4.2.3.0) software focused on impactful SNPs affecting coding sequences, start sites, stop sites, and splice sites, particularly those around the mapping location of *nmz* on linkage group 18. All analyses were performed using the *Danio rerio* GRCz11 reference genome.

Transcriptomic analysis was conducted comparing 5 dpf homozygous *nmz* larvae to homozygous wild-type larvae bred from homozygous wild-type siblings in the same background. Small-eye fish were combined from multiple crosses. Three distinct sets of

crosses were used to generate biological replicates. Similarly, wild-type crosses were used to generate 3 biological replicates for analysis. Total RNA was purified using the RNeasy kit (Qiagen, Germantown, MD, USA). The RNA was shipped to the Next Generation Sequencing Core Facility at the Oklahoma Medical Research Foundation (Oklahoma City, OK, USA), through the Genohub platform. The Oklahoma team performed QC analysis using Kapa qPCR (Roche Technologies, Basel, Switzerland) and the Agilent Tape station (Agilent Technologies, Santa Clara, CA, USA), and prepared polyA-selected libraries using Illumina TruSeq RNA kits (LC Sciences, Houston, TX, USA). HiSeq Rapid Run Illumina (Illumina, San Diego, CA, USA) sequencing was performed and provided approximately 30 million 50 bp single reads per sample. The Oklahoma facility also mapped and annotated the results using the *Danio rerio* GRCz10 genome as the reference. The Epigenetic Core Facility at the University of North Dakota used the DESeq2 workflow to provide the list of differentially expressed (DE) genes included in this paper.

2.4. Cocaine-Induced Conditioned Place Preference (CPP) and Optokinetic Response (OKR)

We used CPP to assess the dopaminergic function of adult fish from the *nmz* and *m863* background. The procedure was conducted as described previously [24,25]. Briefly, sibling fish 8–10 months of age were housed individually for the duration of a three-day test period. On day 1, the fish were transferred to a three-chambered tank and videoed for 10 min using a Top Scan camera array and imaging analysis software suite (CleverSys, Reston, VA, USA). Their preference for each of the three chambers was recorded. The fish were isolated and conditioned in the rear chamber with no drug for 30 min. The next-day baseline preference for all compartments was recorded for 10 min, followed by a second conditioning trial in the rear compartment with or without 10 mg/L cocaine. On the third day, the final preference for all compartments was recorded for untreated and cocaine-treated fish. CPP was determined by subtracting the baseline preference for the rear compartment measured on day 2 from the final preference on day 3.

OKR analysis of adult fish aged 8–10 months old was performed as described by others [26,27]. Fish were temporarily anesthetized in 150 μM tricaine and restrained in a sponge submerged in a clear beaker of fish water. A computer screen was set up such that the fish was at a 45° angle to the screen with the right eye 11 cm from the screen. A program was written in MatLab (version R2023b) to generate a sinusoidal wave grating of vertical black bars on a white background. The grating moved across the screen from the nasal to the temporal visual fields of the right eye. We used two different black bar widths, 2 mm and 8 mm, based on extensive trial and error, but the calculated spatial frequency for both was 0.87 cycles/deg. The grating moved at 0.8 cycles/sec with the illumination at 3500 lux. The goal was to measure the robustness of the response as a measure of visual acuity and perhaps, to a lesser degree, contrast sensitivity. Three 30 s videos were recorded for each fish. The first was a baseline video with no bands cycling across the visual field. The second video recorded the response to the thin bands (2 mm) cycling across the visual field. The third video captured the response to the thicker band (8 mm). Videos were scored by a minimum of three investigators blind to the fish and video trial. Investigators scored the number of track–saccade cycles during the video to measure the robustness of the response. The three observations for each fish and trial were divided by the video lengths and collated to obtain saccades/second.

After CPP and OKR testing, fish were sacrificed to collect brain RNA for future experiments and a tail clip to genotype individuals. Taqman assays were designed to genotype individual 5 dpf larvae and fin clips taken from adult fish (Life Technologies, reference AN9H6FX for *nmz*, and ANT2VDY for *m863*). Individual larvae were anesthetized in tricaine and then transferred to a proteinase K digestion mix (200 mM NaCl, 10 mM Tris,

pH 8.0, 5 mM EDTA, 0.1% SDS and 200 µg/mL proteinase K). After 24 h, the samples were heat-inactivated and diluted. The Taqman assays were performed according to company specifications using a RealTime PCR thermocycler (Biorad, Hercules, CA, USA). To test the genotypes of hybrid larvae, as well as the specificity and efficacy of the Taqman assays, several samples collected were tested with both assays.

2.5. Statistical Analysis

GraphPad Prism (version.10.5.1 Bost, MA, USA) was used for statistical analysis in these experiments. Eye size and body length were measured from homozygous *nmz*, *m863*, and *nmz*/*m863* hybrids. The mutant larvae were compared to wild-type siblings using type 2, two-tailed *t*-tests. Double-blind-assessed OKR scores (saccades/sec) for *nmz* and *m863* adult fish were compared after genotyping, using one-way ANOVA with Bonferroni correction to compare all conditions. For CPP, the second baseline score of percent time spent in the back compartment after conditioning with no drug was compared to the final conditioning trial with or without drug. Fish were genotyped after CPP and OKR testing. As luck would have it, only three heterozygous fish from the *m863* background were in the untreated CPP group. A minimum of 18 were compared for each of the other groups. Similarly, 6 fish were untreated wild type from the *nmz* background, but there was a minimum of 14 in the other groups. One-way ANOVA with Bonferroni's correction was used to compare test groups from each background. OKR scores were compared for each background using repeated measures ANOVA with Bonferroni's correction. A minimum of six fish were used for the *m863* background and a minimum of eighteen were used for each group in the *nmz* background.

The DESeq2 tool was used to generate a table of DE genes. Base means were calculated along with the log base2 fold change in expression in *nmz* mutant fish relative to wild-type fish. A standard deviation was calculated for the log base2 fold change. Dividing the change by the standard deviation generated a Wald test statistic (stat in Table 1 and in Supplementary Table S1). A standard *p*-value and a *p*-value adjusted for the false discovery rate using the Benjamini–Hochberg method (p-adj) were used. The stat numbers were negative if the gene was downregulated in *nmz* and positive if it was upregulated in *nmz*. Functional clustering was performed using the DAVID Bioinformatics website tool (final access date 1 August 2025 National Institutes of Health, https://davidbioinformatics.nih.gov/) with default medium standards. We included all DE genes with an adjusted *p* value lower than 1.0×10^{-3}, or 601 in total (listed in Supplementary Table S1). The DAVID Bioinformatics website was able to assign 495 of these 601 genes for functional clustering.

Table 1. List of CMZ and tp53-associated genes differentially expressed in *nmz*. The ranking is out of the top 601 genes with adjusted *p*-values lower than 0.001. The full list is in the Supplementary Materials.

CMZ Genes	Rank	Stat	Adj. P	tp53 Genes	Rank	Stat	Adj. P
Name				Name			
foxn4	1	−10.15	4.5×10^{-20}	*tp53*	8	8.48	3.8×10^{-14}
dlb (*deltab*)	2	−9.43	2.1×10^{-17}	*gadd45aa*	16	7.44	8.3×10^{-11}
dla (*deltaa*)	4	−9.19	1.3×10^{-14}	*phlda3*	23	6.97	3.1×10^{-12}
her 2	43	−6.42	4.4×10^{-8}	*rap2b*	25	6.88	3.2×10^{-9}
pax6a	51	−6.26	1.0×10^{-7}	*mdm2*	42	6.43	4.2×10^{-8}
neurog1	55	−6.18	1.6×10^{-7}	*casp8*	71	5.97	4.6×10^{-7}

Table 1. *Cont.*

CMZ Genes	Rank	Stat	Adj. P	tp53 Genes	Rank	Stat	Adj. P
Name				Name			
pou4f2	68	−6.0	3.9×10^{-7}	*ccng1*	74	5.93	5.5×10^{-7}
atoh7	80	−5.88	6.9×10^{-7}	*apaf1*	195	5.08	2.6×10^{-5}
ascl1a	152	−5.36	7.6×10^{-6}	*tnfrsf* (*tnfaR*)	403	4.40	3.7×10^{-4}
vsx2	462	−4.30	5.3×10^{-4}	*cdkn1a* (*p21*)	572	4.12	1.0×10^{-4}

3. Results

3.1. Characterization of the nmz Phenotype

Adult poikilothermic vertebrates have a neurogenerative capacity that far exceeds that seen in homeothermic vertebrates [2]. In a previous study, to uncover the regulatory mechanisms underlying this capacity, we employed a forward genetics approach in zebrafish. We generated ENU-mutagenized families and screened at 5 dpf for recessive mutations in F_3 larvae, leading to defects in eye morphology [10]. We were particularly interested in the state of the retinal CMZ. One of these recessive mutants, which we named *no marginal zone* (*nmz*), had a normal body length, but very small eyes that had a dilated appearance compared to those of their wild-type siblings (Figure 1A,B).

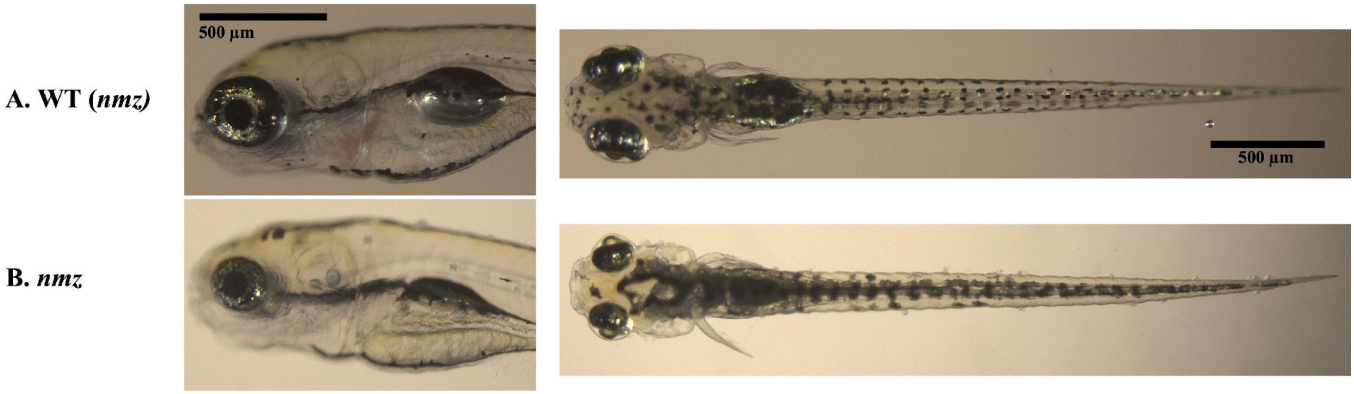


Figure 1. The 5 dpf zebrafish larvae, including wild-type (**A**) and homozygous *nmz* mutant zebrafish (**B**). The homozygous mutant fish had significantly smaller eyes but the same body length as their wild-type siblings.

We performed histology on 5 dpf larvae to assess the morphology and overall health of the eye (Figure 2A,B). While the eye was considerably smaller, there was obvious layering that suggested that the early development of the central retina was relatively normal. Closer inspection at a higher magnification revealed that the CMZ of the *nmz* mutant was reduced and cells were enlarged with nuclei that appeared fragmented (compare the insets of Figure 2A′,B′). In addition, we saw that there appeared to be an expansion of pigmented cells, similar to marginal-zone mutants reported by another group that conducted a similar screen [11]. We saw more evidence of this by looking at the EM level (Figure 3). Wild-type retinae showed very little evidence of dying cells and clear signs of cell division near the pigmented cells around the CMZ (see the arrows in Figure 3B,D and descriptions of cells 1, 2 and 3 in panel D). In contrast, apoptotic cells were readily seen in the CMZ of *nmz* larva (asterisk in Figure 3C,E, and Supplementary Figure S1D). This suggested the

possibility that retinal progenitor cells of the CMZ were compromised while being added to the differentiated retinal tissue in *nmz*.

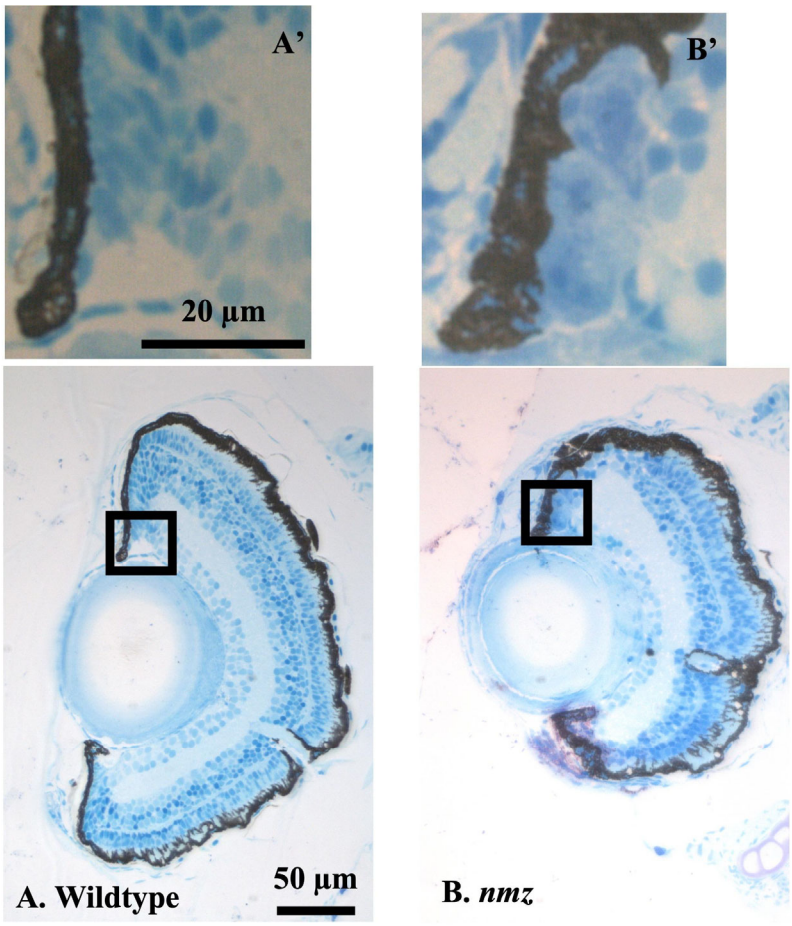


Figure 2. Eye histology at 40× magnification of 5 dpf zebrafish larvae including wild-type (**A**) and homozygous *nmz* mutant zebrafish (**B**). The dorsal CMZ regions outlined by black boxes in A and B are shown immediately above at 63× magnification (**A'**,**B'**). In contrast to the numerous, elongated CMZ cells of the wild-type retina, the mutants have fewer cells that tend to be broader and look more quiescent in appearance. In many instances, there are fragmented nuclei, indicative of cell death.

We tested this possibility with a BrdU pulse-chase experiment (Figure 4). We incubated 3 dpf larvae with BrdU for 24 h, rinsed and changed the water at 4 dpf, and collected and assessed BrdU with immunohistochemistry at 5 dpf (24 h wash out). Wild-type fish showed 1 or 2 wedges of BrdU-labeled cells within the peripheral retina (Figure 4A). Labeling varied, and we did not always see two wedges. Further, Figure 4 shows that the dorsal CMZ has two wedges, while the ventral has one. In other fish, the ventral CMZ was labeled, but not the dorsal CMZ. We suggest that, perhaps, two cell populations dividing at different rates were labeled during the pulse incubation period. In contrast, any labeled cells in the *nmz* mutant never exited the peripheral-most CMZ (Figure 4B). We include additional images of the wild-type and *nmz* mutant BrdU-treated larvae in Supplementary Figure S2 to provide a sense of labeling variation.

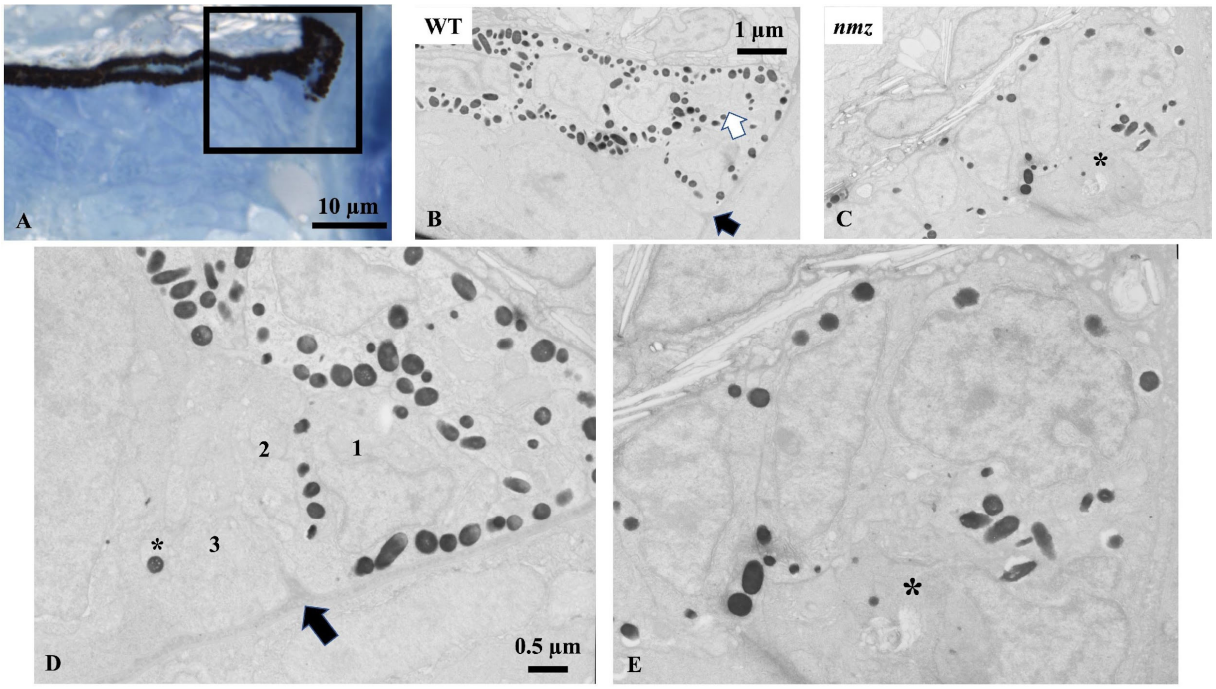


Figure 3. Electron microscopy (EM) of the CMZ in wild-type and *nmz* 5dpf larvae. The central top image, (**A**), is a 100× light microscope picture of the CMZ from a 5 dpf wild-type larva provided for orientation of the EM panels. (**B**,**D**) show the CMZ in a wild-type larva at different magnifications. The white arrow highlights the peripheral RPE. The black arrow shows a cleavage furrow indicative of dividing cells. Numbered cells in (**D**) include a non-dividing RPE cell, with an intact nucleus, at the corner of the CMZ (cell 1). Cells 2 and 3 are associated with the furrow (black arrow), with cell 2 only partly in view. Cell 3, a presumptive retinal stem cell, also has a melanosome (*). (**C**,**E**) show the CMZ of a *nmz* larva at different magnifications. The asterisk in E highlights a cell with a nucleus that is beginning to fragment, indicating probable apoptosis.

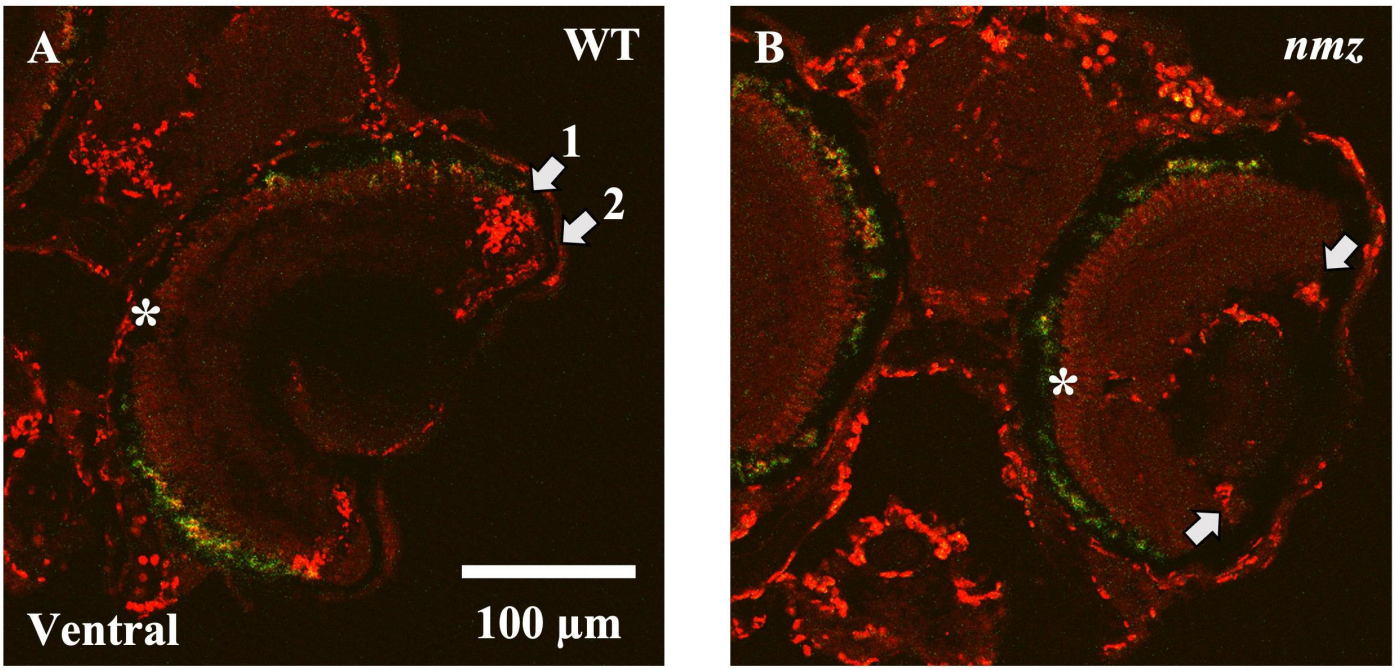


Figure 4. BrdU pulse-chase labeling of wild-type and *nmz* mutant larvae. Fish were exposed to BrdU for 24 h starting at day 3. After rinsing, the larvae were allowed to develop for an additional 24 h,

to 5 dpf. The asterisks mark the optic nerve used as a reference. The arrows point to populations of cells derived from those labeled earlier. Wild-type larvae (**A**) often showed two cell groups, a bigger, centrally located wedge (arrow labeled 1), and a second smaller, more peripheral group (arrow labeled 2). The *nmz* larvae (**B**) showed only a peripheral group of labeled cells (arrow) with no cells in the more central retina. The red staining is BrdU and the green stain shows newly developed rod photoreceptors labeled with a monoclonal antibody called 1D1 (a generous gift from Dr. James Fadool, Florida State University).

3.2. Identification of the Mutation in the ddb-1 Gene Underlying the nmz Phenotype

To identify the mutated gene underlying the *nmz* phenotype, we performed SSLP mapping and found the mutation tightly linked to two markers, z5321 and z1201. This placed the candidate gene around 72 cM on linkage group 18 of the MGH mapping panel. We then compared the genomic sequence of the *nmz* heterozygote and wild-type siblings, focusing on potentially impactful SNPs in that region of LG 18. The most obvious candidate was an SNP predicted to affect splicing between exons 9 and 10 of the ddb-1 gene. We cloned and sequenced a genomic fragment spanning intron 9 and verified that the guanine at the junction between exon 9 and intron 9 was changed to an adenine (Figure 5B). Cloning and sequencing a cDNA fragment covering the splice site between exons 9 and 10 indicated abnormal splicing. In the *nmz* mutant part of the 3′-end of intron 9 joined to an atypical acceptor site further 5′ in exon 9. The result was the introduction of a phase shift in the downstream nucleotides that included a pre-mature stop codon (Figure 5B).

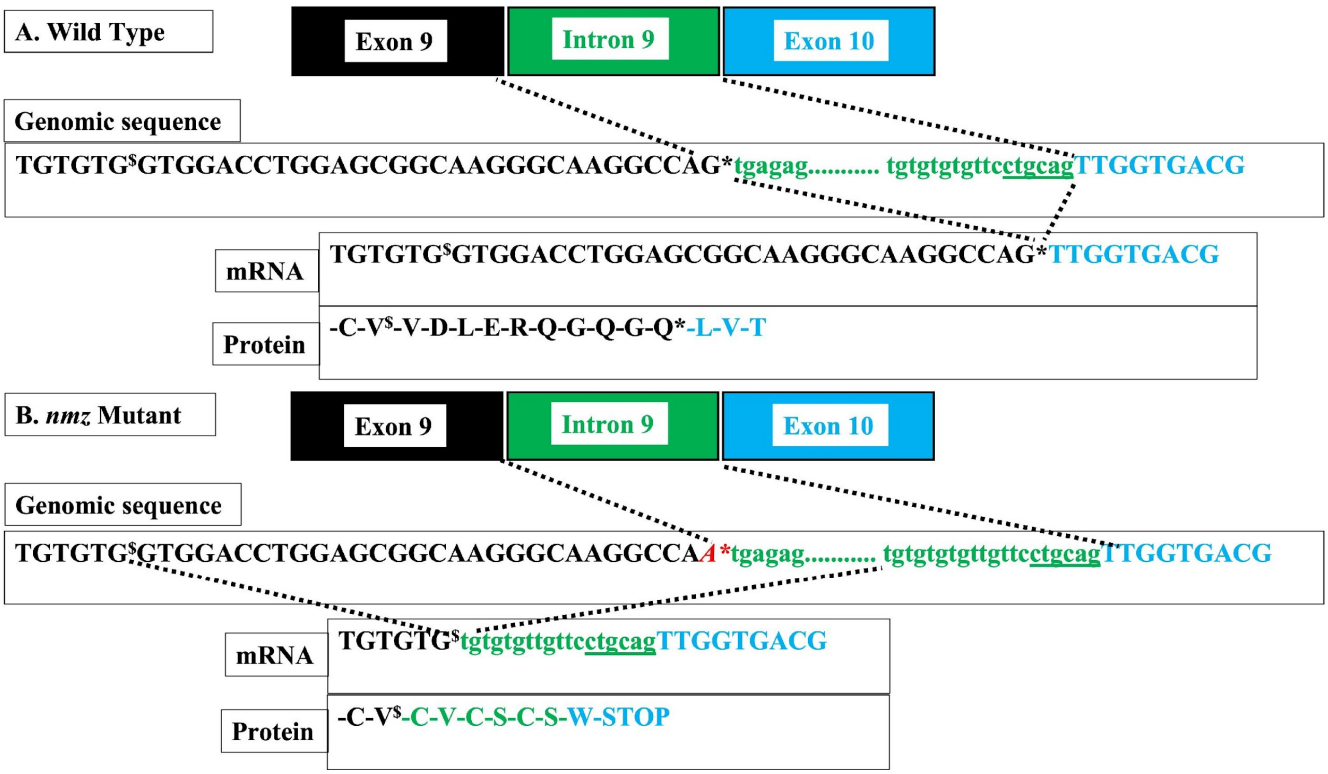


Figure 5. The wild-type sequence in (**A**) is compared to the *nmz* mutation in the ddb-1 gene (**B**). The *nmz* mutation substitutes an A (red italicized A*) for the normal G at the junction between exon 9 and intron 9 (G*). Splicing in the mutant is abnormal, linking a part of the 3′-end of intron 9 to an atypical acceptor site in exon 9 (marked by G$). The result is a phase shift in the mRNA sequence that includes a premature stop site.

At this point, we noticed an earlier publication describing the characterization of another zebrafish line, *m863*, with a mutation in ddb-1 [12]. This group isolated the mutant

while screening for dopamine cells in the brain but reported that it also had very small eyes and an obvious reduction in the CMZ. We were able to obtain this line to perform complementation analysis (thanks again to Dr. Wolfgang Driever). The *m863* mutant was very similar to *nmz* in morphology (Compare Figure 6B with Figure 1B). We measured body length and eye diameter and found that both homozygous mutants had significantly smaller eye diameters than their wild-type siblings (Figure 7A). Average body length, however, was statistically equivalent to their wild-type siblings (Figure 7B). When *m863* heterozygotes were crossed with *nmz* heterozygotes, a small-eye phenotype was seen that was indistinguishable from the two parental lines (Figures 6C and 7). Histological examination of *m863* and the mutant hybrid revealed that the CMZ phenotypes were very similar to those in *nmz* (Figure 8B,C compared to Figure 2B). Persistence of the CMZ phenotype in the hybrid verified that the *nmz* and *m863* phenotypes resulted from mutations in the same gene, ddb-1.

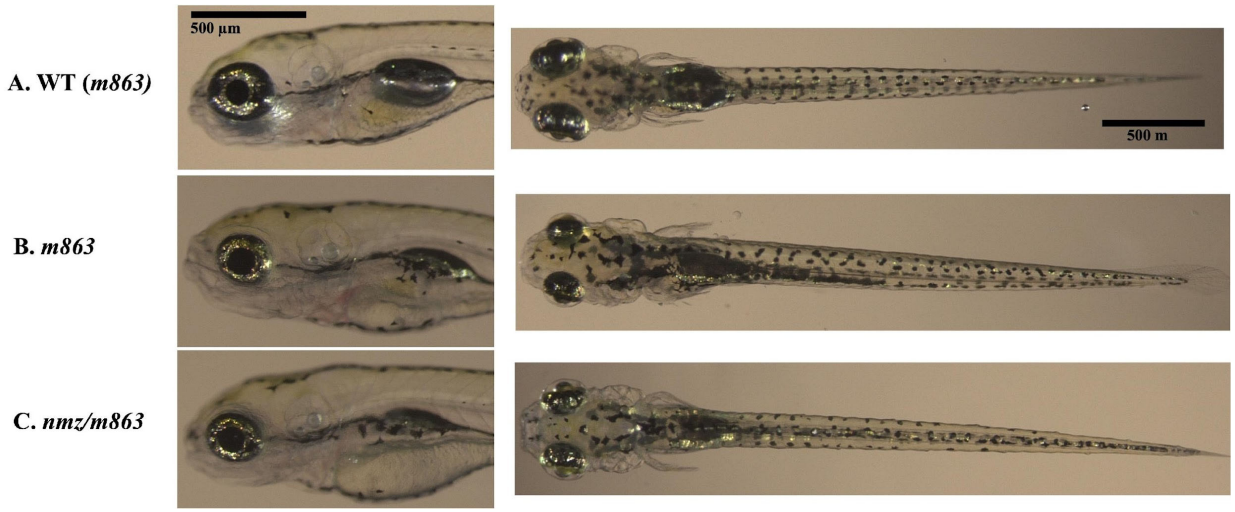


Figure 6. The 5 dpf zebrafish larvae, including the wild-type (**A**), homozygous *m863* mutant (**B**), and hybrid heterozygous zebrafish (**C**), for both the *nmz* and *m863* mutations. The hybrid mutant fish had the same eye diameter and body length as the homozygous mutants (see Figure 7).

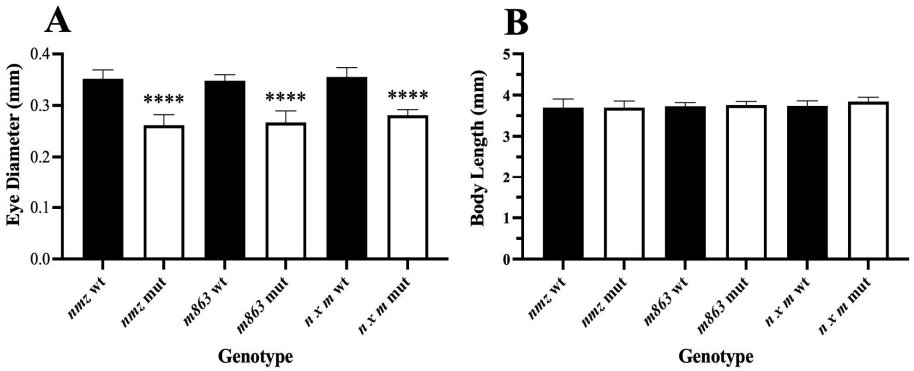


Figure 7. Quantification of body length (**B**) and eye diameter (**A**) for 5 dpf zebrafish larvae. The graphs compare wild-type and homozygous mutant fish from the nmz line and the m863 line. Also shown are hybrids derived from crossing nmz and m863 heterozygous fish (n x m). Eye diameters of the two homozygous fish and hybrids were significantly smaller than those of the wild-type fish (**** $p < 0.0001$). There were no significant differences seen between any group in body length.

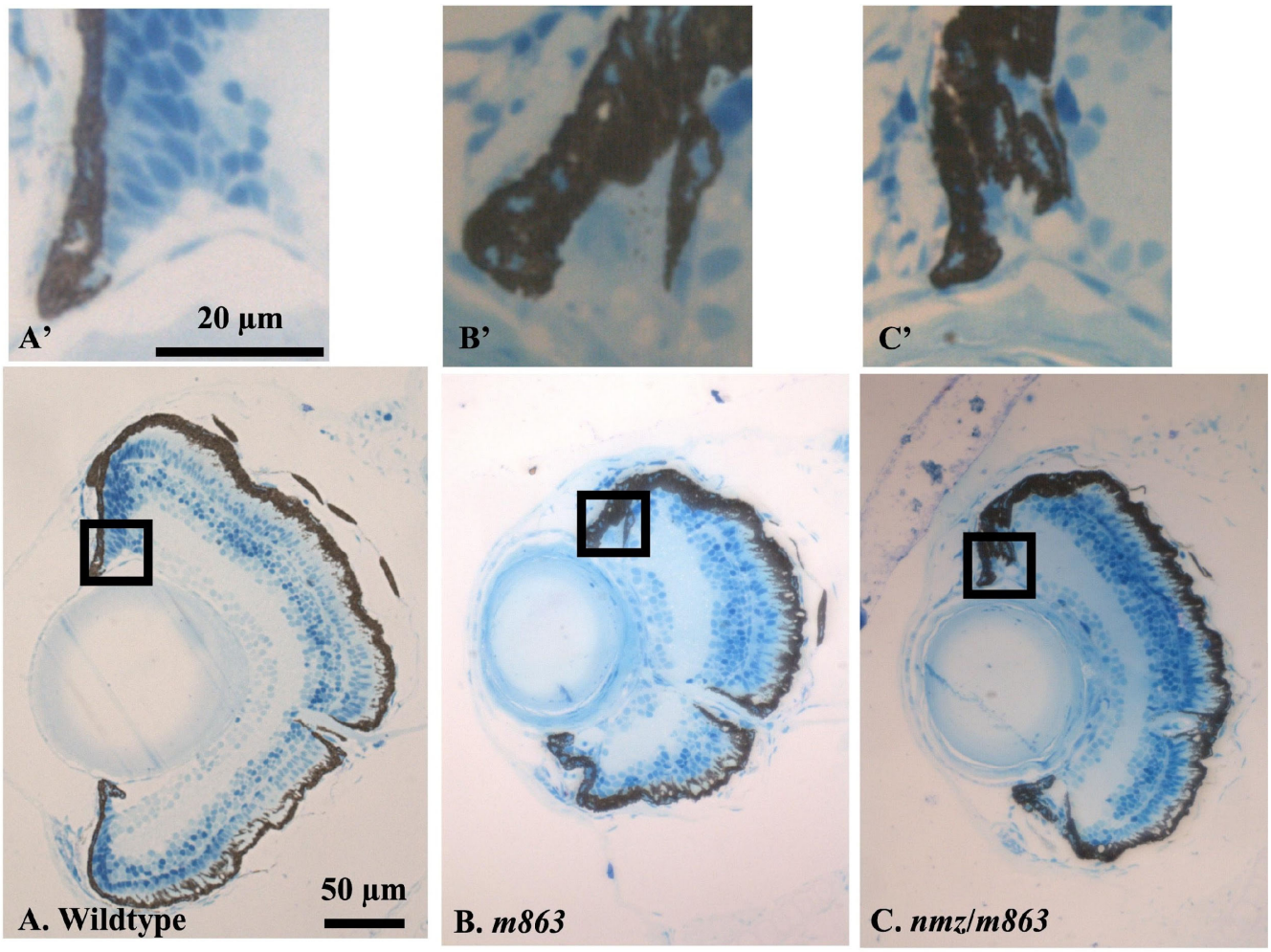


Figure 8. Eye histology at 40× magnification of 5 dpf zebrafish larvae including the *m863* wild type (**A**), homozygous *m863* mutant (**B**) and *nmz*/*m863* hybrid (**C**). The dorsal CMZ regions outlined by black boxes in (**A**–**C**) are shown immediately above at a higher magnification (**A′**–**C′**). The CMZ is similarly reduced in the *nmz* homozygote (Figure 2B), the *m863* homozygote (**B**) and the *nmz*/*m863* hybrid (**C**), suggesting that both mutations are in the same gene.

3.3. Examination of Dopamine-Related and Visual Phenotypes in Heterozygous ddb-1 Mutant Fish

The *nmz* and *m863* homozygous larvae are of a normal length and often start inflating a swim bladder by 5 dpf, but rarely live past 10 dpf. The two lines, however, are readily maintained because heterozygous fish appear normal. Since *m863* was originally screened as a mutation affecting the dopamine neuron number, we asked if the heterozygous adults had abnormal dopamine function. We thus tested fish for dopaminergic function by assessing cocaine-induced conditioned place preference (CPP). Given the homozygous eye phenotype, we also asked if the visual function of the heterozygous adults was compromised by possible ddb-1 gene dosage effects. We thus subjected adult fish to a visual test assessing optokinetic response (OKR) to two computer-generated vertical bar gratings. After testing for CPP and OKR, we genotyped the fish, and looked for differences in response based on heterozygosity in the *nmz* or *m863* mutations.

The CPP responsiveness of *nmz* and *m863* heterozygous fish was not significantly different from that of their respective homozygous wild-type siblings (Supplementary Figure S3). This suggests that the mutation did not affect CPP in heterozygous fish. However, the two mutant lines behaved differently. The *nmz* line was completely unresponsive to cocaine, but again, this was not dependent on the mutation (Supplementary Figure S3A). In contrast to *nmz*, the *m863* line displayed CPP in a way that was quantitatively very

similar to what we have reported for wild-type lines in past studies [24,25]. Homozygous wild-type fish from the *m863* background were not different in responsiveness than the heterozygous fish with the mutation (Supplementary Figure S3B).

Similarly, heterozygous fish from both lines showed no differences from wild-type siblings in OKR (Supplementary Figure S4). However, the two backgrounds differed in OKR. The *nmz* line showed a higher baseline saccade-like movement than the *m863* background (Supplementary Figure S4A vs. B). Closer re-examination of the *nmz* videos revealed that the background eye movements appeared more random and less rhythmic than the regular track–saccade cycle seen in response to the moving bars. However, since all three investigators scored them equally initially, the baseline eye movements could not be excluded. The high background made it difficult to assess OKR to the moving bars, although wild type fish showed a slightly higher response than the baseline (Supplementary Figure S4A). This strange baseline responsiveness was most likely due to genetic background differences rather than the ddb-1 mutation, since wild-type and heterozygous *nmz* fish were nearly identical in score. The *m863* fish showed a low baseline and responded more robustly to the thin bar (Supplementary Figure S4B). Oddly, response to the wider bar was not significantly different than the baseline. It is possible that the thicker stripe was too wide at this spatial frequency and/or temporal frequency to elicit an OKR from the fish. Unfortunately, with the timing of CPP testing, OKR testing, and sacrifice for genotyping and RNA analysis, we could not re-test the fish with a higher spatial or temporal frequency. Despite the low response to the thick bars, the fish showed a statistically significant response to the thin bars. There was no difference between *m863* heterozygous fish and homozygous wild types in OKR. This suggests that as with the *nmz* line, any irregularity in *m683* response was not due to the ddb-1 mutation.

3.4. Transcriptomic Analysis of the nmz Mutant

We performed transcriptomic analysis comparing 5 dpf *nmz* homozygous larvae to wild-type larvae. We have included the top 601 DE genes, with adjusted *p*-values less than 0.001, in Supplementary Table S1. Functional clustering using the DAVID bioinformatics website showed the greatest enrichment for DNA binding (103 of 495 genes, Adj. P = 1.5×10^{-17}) and transcriptional activity (76 genes with adj. p = 2.8×10^{-15}). Nervous system development also proved to be significantly enriched (with 41 genes and an Adj. P = 6.5×10^{-11}). The *m863* mutant line was found to express high levels of tp53 mRNA and other genes associated with tp53 function [12]. In *nmz*, the tp53 signaling pathway was also found to be enriched, with 12 out of 495 genes, and an Adj. P = 5.4×10^{-4}. For convenience and emphasis, in Table 1, we show two subsets of DE genes. The first set includes genes reported by other groups to be expressed in the CMZ [1–7]. All of these CMZ were down regulated (negative stat scores in Table 1). We do call these "CMZ genes" with considerable caution. Most are general neurogenic and neurodifferentiation genes. We assessed whole larvae, so that the change in expression of these genes would not necessarily be limited to the retina or the CMZ. The second set included genes classically associated with tp53 signaling. Similarly to what was reported for *m863*, *nmz* showed elevated expression of tp53-related genes, including tp53 itself (positive stat scores in Table 1). These combined findings suggest that loss of ddb-1 induces cell cycle arrest and apoptosis at the expense of neuronal development in the peripheral retina, and they are consistent with our histological observations. Again, because we examine whole larvae, we exercise caution when interpreting these data, since tp53 is ubiquitously expressed and a differential expression may include several tissues, including the CMZ.

4. Discussion

The Ddb-1 gene encodes a protein with central roles in regulating UV-damage repair of DNA and cell cycle progression [13,14]. The Ddb-1 protein complexes with Cullin 4A and its associated factors to form CRL4, which functions as an E3 ubiquitin ligase. There is evidence that CRL4 regulates activation of the Tp53, which in turn regulates cell cycle progression and apoptosis [28–30]. Normally, Tp53 levels are low because the Mdm2-mediated ubiquitin ligase complex rapidly targets it for degradation [16]. Cellular stress initiated by chemical or UV insult inhibits Mdm2 activity by a number of mechanisms and thus increases Tp53 stability. Since Tp53 is a transcription factor that autoregulates, the increased stability also increases Tp53 transcript levels. In turn, Tp53 regulates the expression of many target genes that can initiate cell cycle arrest and/or apoptosis. There is evidence that some forms of the CRL4 complex act similarly to Mdm2 and regulate Tp53 stability by targeting it for degradation [9]. There is also evidence that CRL4 can regulate Mdm2 activity indirectly by controlling ribosome biosynthesis [28,29]. Certain ribosomal proteins bind to and inhibit the Mdm2 ubiquitination of Tp53, thus increasing its stability. This may explain the observation by many groups that loss of Ddb-1, and presumably, as a result, CRL4 function, leads to an increase in Tp53 expression, with wide-ranging developmental effects [12,18,19].

Elimination of Ddb-1 in mice results in lethality by E12.5 [18]. More selective deletion in the brain was still lethal and the investigators reported elimination of proliferating populations of neural progenitors along with evidence of extensive apoptosis [18]. The effect of Ddb-1 elimination on these neural precursors was partially mitigated by suppression of Tp53. Similarly, fetal hematopoiesis was found to be dependent on Ddb-1 in mice [19]. In that study, selective silencing of Ddb-1 led to a rise in the Tp53-mediated apoptosis of hematopoietic precursors. In the study characterizing the ddb-1 mutation in the *m863* zebrafish line, the investigators also reported a similar connection to tp53 signaling and hypothesized that this led to genomic instability, cell cycle arrest, and apoptosis in neural stem cell niches, including the CMZ, and dopaminergic systems of the brain [12]. Our findings for *nmz* are consistent with this connection of ddb-1 elimination with tp53-directed cell cycle disruption and apoptosis in the CMZ.

Regulation of cell cycle progression and apoptosis by Tp53 is very complex and involves activation of distinct sets of effectors (recently reviewed in [16,17]). Apoptosis is stimulated by Tp53 in two general pathways, called intrinsic and extrinsic. Tp53 drives the intrinsic pathway by increasing the expression of BH-3 proteins, including Puma and Noxa. These inhibit Bcl-2, thus activating the Bax/Bak cascade of protein interactions, which leads to caspase-mediated cell destruction. The extrinsic pathway involves the binding of ligands to so-called death receptors on the cell membrane. Ligand binding activates a signaling cascade and induces the formation of an intracellular death-inducing-signaling-complex (DISC). The DISC recruits Casp8, which then initiates a further cascade of caspase activation that leads to cell death. The central role of Tp53 in this process involves the increasing expression of death receptors like the Fas and Tnf-a receptors as well as intracellular components like Casp8. Tp53 stimulates the expression of other genes including Gadd45 and Cdk1 (p21), which can arrest the cell cycle at the G2/M stage and trigger apoptosis [31,32].

In the *nmz* mutants, the absence of ddb-1 stimulates tp53 expression in a manner similar to that described in other studies, including the work with the *m863* zebrafish mutant [12,18,19]. As reported by others, the loss of ddb-1 results in the appearance of apoptotic cells, as indicated by TUNEL assays in the zebrafish brain and eye, including the CMZ [12]. We saw several tp53-regulated genes that were transcriptionally upregulated in *nmz*, including gadd45a and cdkn1a (p21), tnfrsf (tnfa receptor), and casp8. Caution

must be exercised here, because the tp53 pathway is also regulated extensively post-transcriptionally, but this combination of gadd45a and cdkn1a upregulation has been most closely associated with cell cycle arrest at the G2/M boundary, while tnfrsf and casp8 are linked to the extrinsic apoptotic pathway [16,17]. It is tempting to speculate that crosstalk between the two tp53-regulated processes results from the loss of ddb-1 in the CMZ of the *nmz* mutants. However, this transcriptomic analysis was on whole embryos, and without further CMZ-specific validation of these tp53-regulated genes, strong conclusions must be viewed with caution.

Our additional observations described herein support previous work elegantly outlining the retinogenic process at the CMZ [1,3]. First, cells are generated at the lateral edge of the CMZ, where there is proximity to the future ciliary epithelium, RPE, circumferential vitreal blood vessels, and the lens. Initial expansion of the CMZ is relatively slow, involving asymmetric divisions of retinal stem cells at the very periphery. These are the rx2-positive stem cells described by others [3]. We speculate that these make up the peripheral-most CMZ population of BrdU-positive cells in our pulse chase experiments (arrow 2 in Figure 4A). Because of the variation in labeling patterns in the pulse-chase experiments (Supplementary Figure S2), we suspect that the labeling of those early stem cells was infrequent, but we also cannot fully exclude tnfaartifacts arising from the angle of sectioning. Looking at the finer histology and electron microscopy in the CMZ, we saw numerous examples where it appeared that the CMZ had retinal stem cells and/or progenitor cells, with elongated nuclei, that also had melanosomes (Figure 3D and S1C). It is tempting to argue that CMZ retinal stem cells might result from an earlier asymmetric division of a pigmented precursor. It is worth noting that we have noticed an apparent increase in the number of pigmented cells in the CMZ, although we cannot rule out the smaller dimension of the *nmz* eye, distorting the RPE and presumptive ciliary epithelium. In this way, the *nmz* perhaps falls in the Class 1C mutants described in similar work by another laboratory that screened for CMZ mutants [11].

Slow asymmetric division of the retina stem cells gives rise to a second, faster expansion of the retinal progenitor cells [1,3]. These cells express rx2 and pax6a, along with various delta-notch pairs. We suspect that these are the cells we see in the second more centrally located cell cluster after BrdU pulse-chase (1st arrow in Figure 4A). The retinal progenitors form a wedge or arched stripe [3] that eventually fully differentiates into all retinal cell types. It is tempting to speculate that these wedges comprise functionally linked circuits representing discrete expansions of the peripheral visual field as the eye grows.

Our data seems to suggest that the ddb-1 mutation affects the rapid secondary expansion, rather than the slow earlier expansion (Figure 4B), but not necessarily. Others have shown that ddb-1 is ubiquitously expressed in the early zebrafish embryo but becomes more restricted later [11]. The *nmz* and *m863* phenotypes do not start becoming apparent until 3 dpf. The investigators who characterized the *m863* mutant demonstrated that ddb-1 was maternally expressed and argued that this maternal expression rescued any earlier phenotype [11]. Screening the ddb-1 mutation phenotype probably reflects the tissues normally proliferating rapidly during the maternal to zygotic transition (MZT, [33]). At the MZT, maternally derived ddb-1 transitions to that exclusively provided by the larval fish. In the mutant lines, cell proliferation and development are essentially arrested by 5 dpf, but structures developed before the transition at 3 dpf look relatively normal. This points to a central caveat of screening for stem cell mutants in this type of experiment. Maternal rescue can mask the early ubiquitous effects of housekeeping genes, making the mutation seem specific for a particular organ or tissue. Finally, we concede that since we conducted transcriptome analysis on whole larvae, rather than the isolated retina, we must view these conclusions with caution.

We tested fish heterozygous for the ddb-1 mutations to see if there were any subtle changes in dopaminergic and visual function. We used CPP to test dopaminergic function. The *nmz* and *m863* lines showed different sensitivities to cocaine. The *nmz* line, which was insensitive to the drug, is highly inbred, much more so than the *m863* line, which had physical traits of multiple zebrafish strains. During the *nmz* line's history, they may have lost drug sensitivity randomly through inbreeding. In contrast, the *m863* fish behaved normally in the CPP test. The basis for the difference in sensitivity between the two lines was not due to the ddb-1 mutation, as wild-type and heterozygous fish showed no difference in sensitivity.

OKR was used to assess visual function. Again, the mutant lines behaved differently. The *nmz* fish showed much more spontaneous eye movements, even without any grating stimulus. With higher scrutiny, the baseline eye movements did look less rhythmic than with the moving bars, but since we all scored the responses similarly, we left the results as is. We do not have an explanation except that perhaps the *nmz* fish do not see very well and the spontaneous eye movements are due to the resulting agitation in a novel situation. Several earlier experiments using a rotating drum with similar spatial and temporal frequencies also indicated poor OKR in the *nmz* background (unreported observations). Unfortunately, we did not know about the ddb-1 mutation during these earlier experiments and did not genotype the fish at that time. Poorer vision may also have played a role in the low CPP response since the secondary cues in the assay are mostly visual. In contrast, the *m863* fish displayed a low background and a high response to the thin bars. We currently believe that the thicker bands require a higher spatial or temporal frequency to elicit a more robust OKR in fish with normal vision. Regardless of the differences between the two lines, the ddb-1 mutations were clearly not related to visual function, as both wild type and heterozygous fish in each background showed very similar responses.

5. Conclusions

In conclusion, the ddb-1 gene probably serves ubiquitous, housekeeping roles in DNA repair and cell cycle regulation. This study provides another example highlighting ddb-1 function in maintaining neural stem cell populations. The loss of ddb-1 in the *nmz* mutant is particularly apparent in the regulation of the CMZ. This supports earlier studies on the *m863* zebrafish mutant and others in transgenic models. These studies all point to the role of ddb-1 in regulating the expression and function of tp53 and related genes. In the *nmz* mutants, loss of ddb-1 correlates with an increase tp53 expression, cell cycle arrest and cell death. Heterozygosity for the ddb-1 allele seems to have no detrimental effects on vision or behavior.

Supplementary Materials: The following supporting information can be downloaded at https://www.mdpi.com/article/10.3390/fishes10110539/s1: Figure S1: Additional histology and EM of the CMZ in wild-type and *nmz* 5 dpf larvae; Figure S2: Other examples of BrdU pulse-chase results in mutant and wild-type *nmz* fish; Figure S3: CPP behavior for wild-type fish and fish heterozygous for the *nmz* and *m863* mutations; Figure S4: OKR behavior for wild-type fish and fish heterozygous for the *nmz* and *m863* mutations; Table S1: Genes differentially expressed in the *nmz* mutant with an adjusted *p*-value less than 0.001.

Author Contributions: Conceptualization, supervision, funding acquisition and primary draft preparation was performed by T.D. Investigation, performance of experiments, and establishment of methodology was a combined effort for all the authors K.J., A.G., T.A., T.B., M.K.G., C.L.J., J.G., C.K.O., L.R. and T.D. Most of the final version of formal analysis was the responsibility of T.D., but all the authors analyzed and presented data, including K.J., A.G., T.A., T.B., M.K.G., C.L.J., J.G., C.K.O. and L.R. All the authors contributed to reviewing and editing the final submitted draft: K.J., A.G.,

T.A., T.B., M.K.G., C.L.J., J.G., C.K.O., L.R. and T.D. All authors have read and agreed to the published version of the manuscript.

Funding: This research was supported in part by a National Science Foundation REU Site award, 1852459. This work was also supported by the National Institute of General Medical Sciences of the National Institutes of Health under Award Number U54GM128729 and Award number P20GM104360.

Institutional Review Board Statement: IACUC IACUC2307-0047 2023-10-10.

Data Availability Statement: The original contributions presented in this study are included in the article/Supplementary Material. Further inquiries can be directed to the corresponding author.

Acknowledgments: We want to acknowledge the Genohub platform, the Oklahoma Medical Research Foundation NGS Core, and Admera Health Biopharma Services for superior sequencing and bioinformatics support. We want to thank Ella Tkach for providing assistance in maintaining the zebrafish colony at UND. We would like to thank Wolfgang Driever at the University of Freiberg, Germany, for generously sharing the *m863* mutant zebrafish strain with us. We also want to thank Adam Scheidegger of the UND epigenetics core for assembling the list of DE genes in the *nmz* mutant. We would like to thank James Fadool at Florida State University for sharing the 1D1 antibody with us. We want to thank John Matsui for his excellent technical assistance in the Harvard electron microscopy core facility. We would like to thank and acknowledge Brian Link, a superior scientist and colleague, who led the mutagenesis and screening experiments at Harvard University that generated the *nmz* mutant. Finally, we want to thank John E. Dowling, an exemplary scientist, mentor and person, in whose laboratory these studies began.

Conflicts of Interest: The authors declare no conflicts of interest.

References

1. Raymond, P.A.; Barthel, L.K.; Bernardos, R.K.; Perkowski, J.J. Molecular characterization of retinal stem cells and their niches in adult zebrafish. *BMC Dev. Bio.* **2006**, *6*, 36. [CrossRef]
2. Ail, D.; Perron, M. Retinal degeneration and regeneration-lessons from fishes and amphibians. *Curr. Pathobiol. Rep.* **2017**, *5*, 67–78. [CrossRef]
3. Wan, Y.; Almeida, A.D.; Rulands, S.; Chalour, N.; Muresan, L.; Wu, Y.; Simons, B.D.; He, J.; Harris, W.A. The ciliary marginal zone of the zebrafish retina: Clonal and time-lapse analysis of a continuously growing tissue. *Development* **2016**, *143*, 1099–1107. [CrossRef]
4. Fischer, A.J.; Reh, T.A. Identification of a proliferating marginal zone of retinal progenitors in postnatal chickens. *Dev. Biol.* **2000**, *220*, 197–210. [CrossRef]
5. Tropepe, V.; Coles, B.L.K.; Chiasson, B.J.; Horsford, D.J.; Elia, A.J.; McInnes, R.R.; van der Kooy, D. Retinal stem cells in the adult mammalian eye. *Science* **2000**, *287*, 2032–2036. [CrossRef]
6. Fischer, A.J.; Bosse, J.L.; El-Hodiri, H.M. Reprint of: The ciliary marginal zone (CMZ) in development of the vertebrate eye. *Exp. Eye Res.* **2014**, *123*, 115–120. [CrossRef]
7. Driever, W.; Sonica-Krezel, L.; Schier, A.F.; Neuhauss, S.C.F.; Malicki, J.; Stemple, D.L.; Stainier, D.Y.R.; Zwartkruis, F.; Abdelilah, S.; Rangini, Z.; et al. A genetic screen for mutations affecting embryogenesis in zebrafish. *Development* **1996**, *123*, 37–46. [CrossRef]
8. Amsterdam, A.; Burgess, S.; Golling, G.; Chen, W.; Sun, V.; Townsend, K.; Farrington, S.; Haldi, M.; Hopkins, N. A large-scale insertional mutagenesis screen in zebrafish. *Genes Dev.* **1999**, *13*, 2713–2724. [CrossRef]
9. Brockerhoff, S.E.; Hurley, J.B.; Janssen-Bienhold, U.; Neuhauss, S.C.F.; Driever, W.; Dowling, J.E. A behavioral screen for isolating zebrafish mutants with visual system defects. *Proc. Natl. Acad. Sci. USA* **1995**, *92*, 10545–10549. [CrossRef]
10. Link, B.A.; Darland, T. Chapter 40: Genetic analysis of initial and ongoing retinogenesis in the zebrafish: Comparing the central neuroepithelium and marginal zone. *Prog. Brain Res.* **2001**, *131*, 565–577.
11. Wehman, A.M.; Straub, W.; Meyers, J.R.; Raymond, P.A.; Baier, H. Genetic dissection of the zebrafish. retinal stem cell compartment. *Dev. Biol.* **2005**, *281*, 53–65. [CrossRef]
12. Hu, Z.; Hulzschuh, J.; Driever, W. Loss of DDB1 leads to transcriptional p53 pathway activation in proliferating cells, cell cycle deregulation and apoptosis in zebrafish embryos. *PLoS ONE* **2015**, *10*, e0134299. [CrossRef]
13. O'Connell, B.C.; Harper, J.W. Ubiquitin proteasome system (UPS): What can chromatin do for you? *Curr. Opin. Cell Biol.* **2007**, *19*, 206–214. [CrossRef] [PubMed]
14. Iovine, B.; Iannella, M.L.; Bevilacqua, M.A. Damage-specific DNA binding protein 1 (DDB1): A protein with a wide range of functions. *Int. J. Biochem. Cell Biol.* **2011**, *43*, 1664–1667. [CrossRef]

15. Levine, A.J.; Oren, M. The first 30 years of p53: Growing ever more complex. *Nat. Rev. Cancer* **2009**, *9*, 749–758. [CrossRef]
16. Aubrey, B.J.; Kelly, G.L.; Janic, A.; Herold, M.J.; Strasser, A. How does p53 induce apoptosis and how does this relate to p-53-mediated tumour suppression? *Cell Death Differ.* **2018**, *25*, 104–113. [CrossRef]
17. Hafner, A.; Bulyk, M.L.; Jambhekar, A.; Lahav, G. The multiple mechanisms that regulate p53 activity and cell fate. *Nat. Rev. Mol. Cell Biol.* **2019**, *20*, 199–210. [CrossRef] [PubMed]
18. Cang, Y.; Zhang, J.; Nicolas, S.A.; Bastien, J.; Li, B.; Zhou, P. Deletion. of Ddb1 in mouse brain and lens leads to p53-dependent elimination of proliferating cells. *Cell* **2006**, *127*, 929–940. [CrossRef] [PubMed]
19. Gao, J.; Buckley, S.M.; Cimmino, L.; Guillamot, M.; Strikoudis, A.; Cang, Y.; Goff, S.P.P.; Aifantis, I. The Cul4-Dddb1 ubiquitin ligase complex controls adult and embryonic stem cell differentiation and homeostasis. *eLife* **2015**, *4*, e07539. [CrossRef]
20. Knapik, E.W.; Goodman, A.; Ekker, M.; Chevrette, M.; Delgado, J.; Neuhauss, S.; Shimoda, N.; Driever, W.; Fishman, M.C.; Jacob, H.J. A microsatellite genetic linkage map for zebrafish (*Danio rerio*). *Nat. Genet.* **1998**, *18*, 338–343. [CrossRef]
21. Liao, E.C.; Zon, L.I. Chapter 10 Simple Sequence-Length Polymorphism Analysis. *Meth. in Cell Biol.* **1998**, *60*, 181–183.
22. Allwardt, B.A.; Lall, A.B.; Brockerhoff, S.E.; Dowling, J.E. Synapse formation is arrested in retinal photoreceptors of the zebrafish *nrc* mutant. *J. Neurosci.* **2001**, *21*, 2330–2342. [CrossRef] [PubMed]
23. Schmitt, E.A.; Dowling, J.E. Early retinal development in the zebrafish, Danio rerio: Light and electron microscopic analyses. *J. Comp. Neurol.* **1999**, *404*, 515–536. [CrossRef]
24. Darland, T.; Mauch, J.T.; Meier, E.M.; Hagan, S.J.; Dowling, J.E.; Darland, D.C. Sulpiride, but not SCH23390, modifies cocaine-induced conditioned place preference and expression of tyrosine hydroxylase and elongation factor 1a in zebrafish. *Pharmacol. Biochem. Behav.* **2012**, *103*, 157–167. [CrossRef]
25. Mersereau, E.J.; Boyle, C.A.; Poitra, S.; Espinoza, A.; Seiler, J.; Longie, R.; Delvo, L.; Szarkowski, M.; Maliske, J.; Chalmers, S.; et al. Longitudinal effects of embryonic exposure to cocaine on morphology, cardiovascular physiology and behavior in zebrafish. *Int. J. Mol. Sci.* **2016**, *17*, 847–865. [CrossRef]
26. Tappeiner, C.; Gerber, S.; Enzmann, V.; Balmer, J.; Jazwinska, A.; Tschopp, M. Visual acuity and contrast sensitivity of adult zebrafish. *Front. Zool.* **2012**, *9*, 10. [CrossRef]
27. Cameron, D.J.; Rassamdana, F.; Tam, P.; Dang, K.; Yanez, C.; Ghaemmaghami, S.; Dehkordi, M.I. The optokinetic response as a quantitative measure of visual acuity in zebrafish. *J. Vis. Exp.* **2013**, *80*, e50832.
28. Wei, S.; Xing, J.; Chen, J.; Chen, L.; Lv, J.; Chen, X.; Li, T.; Yu, T.; Wang, H.; Wang, K.; et al. DCAF13 inhibits the p53 signaling pathway by promoting p53 ubiquitination modification lung adenocarcinoma. *J. Exp. Clin. Cancer Res.* **2024**, *43*, 3. [CrossRef] [PubMed]
29. Han, X.-R.; Sasaki, N.; Jackson, S.C.; Wang, P.; Li, Z.; Smith, M.D.; Xie, L.; Chen, X.; Zhang, Y.; Marzluff, W.F.; et al. CRL4 E3 ubiquitin ligase controls ribosome biogenesis, cell proliferation and development. *Sci. Adv.* **2020**, *6*, eabd6078. [CrossRef] [PubMed]
30. Liu, Y.; Deisenroth, C.; Zhang, Y. RP-MDM2-p53 pathway: Linking ribosomal biogenesis and tumor surveillance. *Trends Cancer* **2016**, *2*, 191–204. [CrossRef]
31. Sheikh, M.S.; Hollander, M.C.; Fornace, A.J. Role of Gadd45 in Apoptosis. *Biochem. Pharmacol.* **2000**, *59*, 43–45. [CrossRef] [PubMed]
32. Palomer, X.; Salvador, J.M.; Grinan-Ferre, C.; Barroso, E.; Pallas, M.; Vazquez-Carrera, M. GADD45A: With or without you. *Med. Res. Rev.* **2024**, *44*, 1375–1403. [CrossRef] [PubMed]
33. Lee, M.T.; Bonneau, A.R.; Giraldez, A.J. Zygotic genome activation during the maternal-to-zygotic transition. *Annu. Rev. Cell Dev. Biol.* **2014**, *30*, 581–613. [CrossRef] [PubMed]

Disclaimer/Publisher's Note: The statements, opinions and data contained in all publications are solely those of the individual author(s) and contributor(s) and not of MDPI and/or the editor(s). MDPI and/or the editor(s) disclaim responsibility for any injury to people or property resulting from any ideas, methods, instructions or products referred to in the content.